

Using Artificial Intelligence Methods to Classify Different Seismic Events

Tingting Wang¹, Yinju Bian^{*1}, Yixiao Zhang¹, and Xiaolin Hou¹

Abstract

The classification of seismic events is crucial for monitoring underground nuclear explosions and regional unnatural seismic events. To classify tectonic earthquakes, explosions, and mining-induced earthquakes, we established 36- and 60-dimensional network-averaged datasets and single-station datasets through feature extraction and spectral amplitude analysis. Using different artificial intelligence (AI) methods, including the support vector machine (SVM), extreme gradient boosting (XGBoost), long short-term memory network (LSTM), residual neural network, and long short-term memory fully convolutional network (LSTM-FCN), we constructed two-class and three-class models, analyzed the change in the classification with epicentral distances, and evaluated the generalizability of different classifiers. The results showed that the accuracies of different AI models with the feature extraction dataset were higher than those achieved with the spectral amplitude dataset, indicating that the feature extraction method can more clearly highlight the differences between different types of seismic events. The accuracies with the network-averaged dataset were 5%–8% higher than that achieved using the single-station dataset. The earthquake and mining-induced earthquake classifiers constructed by different AI methods had the best performance, followed by the earthquake and explosion classifier, and the explosion and mining-induced earthquake classifier, with average accuracies of 97.4%–98.4%, 96.5%–97.6%, and 88.8%–90.6%, respectively. In the model generalization evaluation, the test accuracies and F1-Scores of the two-class models with the 36-dimensional network-averaged dataset exceeded 90%. Among the five AI methods, XGBoost and LSTM both performed well in classification of different datasets, indicating that these models have good application prospects for seismic event classifications.

Cite this article as Wang, T., Y. Bian, Y. Zhang, and X. Hou (2022). Using Artificial Intelligence Methods to Classify Different Seismic Events, *Seismol. Res. Lett.* **94**, 1–16, doi: 10.1785/0220220055.

Supplemental Material

Introduction

Seismic analysis is regarded as an effective technical approach to monitor long-distance underground nuclear explosions and discriminate them from earthquakes. Scholars have proposed a variety of identification features, such as the $m_b : M_s$ magnitude ratio, the initial motion of P wave, the P -wave complexity, and the P/S amplitude ratio (e.g., Pomeroy *et al.*, 1982; Fisk *et al.*, 2009; Douglas, 2013; Zhao *et al.*, 2017). With the establishment of dense networks of stations worldwide, more low-magnitude earthquakes and unnatural seismic events that occur at local and regional distances will be recorded, and greater effort is needed to classify low-magnitude unnatural seismic events, such as nuclear explosions, industrial explosions, and mining-induced earthquakes (Smith, 1993; Stump *et al.*, 1994). Establishing accurate earthquake catalogs, explosion catalogs, and mining-induced earthquake catalogs is crucial for studying seismic activity and the physical mechanisms of explosions, and for assessing the seismic risk associated with human mining activities.

Theoretically, there is a large difference between the focal mechanism of earthquakes and that of explosions (Ford *et al.*, 2009). Earthquakes generate shear waves, and have a double-couple focal mechanism and four-quadrant amplitude distribution. Industrial explosions occur near the surface, and their high-frequency components decay rapidly along the propagation path. The seismic records of mining-induced earthquakes are relatively complex. For an inward collapse, the initial P -wave motion is downward, and the P/S amplitude ratio has the characteristics of an expansion source (Zhao *et al.*, 1995). There are also some shear-slip components in the mining-induced seismic rock failure process (Kortström *et al.*, 2016). Because of the large distance between stations in most

1. Institute of Geophysics, China Earthquake Administration, Beijing, China,
ID <https://orcid.org/0000-0002-6583-9718> (YB); ID <https://orcid.org/0000-0002-4500-7017> (YZ); ID <https://orcid.org/0000-0001-6052-092X> (XH)

*Corresponding author: bianyinju@cea-igp.ac.cn

© Seismological Society of America

seismic networks and the significant influence of the 3D path effect on high-frequency seismic waves, the source mechanisms of small-magnitude seismic events (e.g., $M_L < 3$) are still difficult to determine (Walter *et al.*, 2018; Tang *et al.*, 2020). Therefore, general event classification methods often extract features from seismic waves (Kim *et al.*, 1997, 2018; Holt *et al.*, 2019). Wang *et al.* (2013) compared several pattern recognition methods and showed that comprehensive recognition based on multiple features can achieve more stable and higher recognition rates than methods based on a single feature.

In the recent years, interest in artificial intelligence (AI) has increased substantially in science and technology, with this branch of computer science showing strong applicability in seismological data processing (Ross *et al.*, 2018; Zhao and Chen, 2019). Many AI studies on seismic event classification have been published; for example, Kuyuk *et al.* (2012, 2014) combined self-organizing mapping and neural networks with unsupervised learning to classify small earthquakes and mine explosions; Kortström *et al.* (2016) used support vector machine (SVM) to classify earthquakes and nonearthquakes using short-term average (STA) values in different frequency bands. Reynen and Audet (2017) used two attributes, the polarization and frequency content, as the input to logistic regression and showed a high accuracy in discriminating between blasts and earthquakes. Wei *et al.* (2019) introduced a residual neural network (ResNet) model in the classification of earthquakes and explosions. Renouard *et al.* (2021) developed two random forest classifiers to discriminate between earthquakes and blasts, and quantitatively explored feature importance for discrimination. Koper *et al.* (2016) proposed using the difference between local magnitude and coda duration magnitude ($M_L - M_C$) as a depth discriminator to discriminate manmade seismic events from tectonic earthquakes. There are a few studies to discriminate mining-induced earthquakes from earthquakes and explosions. Tang *et al.* (2020) used SVM to classify earthquakes, explosions, and mining-induced earthquakes with spectral amplitudes and indicated that the classifier has limited capability in different regions. Thus, the discrimination of induced earthquakes and the universality of discriminant features require further study.

This article mainly focuses on the classification of tectonic earthquakes, explosions, and mining-induced earthquakes in central and eastern China. First, we establish two different datasets: one of which is a 36-dimensional single-station and network-average feature extraction dataset, including amplitude ratio, high- and low-frequency energy ratio, corner frequency, waveform duration, waveform complexity, zero-crossing rate, cepstral complexity, and instantaneous frequency complexity. The other is a 60-dimensional single-station and network-averaged spectral amplitude dataset, in which the data processing is simpler, and the seismic waveform is directly converted into amplitude spectra. Second, five AI methods, including SVM, extreme gradient boosting (XGBoost), long short-

term memory (LSTM) networks, ResNet, and long short-term memory fully convolutional network (LSTM-FCN) are used to build two-class and three-class models between three types of events. Finally, we compare the five AI models through model performance measures, analyze the change in the classification performance with different epicentral distances, and evaluate the generalizability of different classifiers.

Data and Analysis

The 2009–2020 natural earthquake and unnatural seismic event catalogs, which include explosions of various industrial activities and mining-induced earthquakes, were obtained through the earthquake cataloging system, the Beijing Digital Seismic Network, and provincial earthquake monitoring centers in China. The seismic data were obtained from the Data Management Centre of the China National Seismic Network (see [Data and Resources](#); Zheng *et al.*, 2010). In this article, earthquake refers to a tectonic earthquake, explosion refers to a blast generated by industrial activities or a sudden explosion disaster, and mining-induced earthquake refers to an earthquake induced by mining. Compared with tectonic earthquakes, mining-induced earthquakes are usually shallower in depth and more complex in focal mechanism, which may be implosion (mine collapse), double-couple, or a combination of the both (Koper *et al.*, 2016).

First, we individually reviewed the three-component seismic records of unnatural seismic events for event verification. Explosions are characterized by a greater *P*-wave amplitude than that of the *S* wave, an upward initial *P*-wave motion, and Rayleigh-wave development. In contrast, mining-induced earthquakes are characterized by a downward initial motion (mine collapse), Rayleigh waves, and low-velocity guided wave development (Zhao *et al.*, 1995; Koper *et al.*, 2016). The nature of an event is further confirmed by comparison with the waveforms of well-defined seismic event types and locations, for example, a large quarry area and mining area. Second, the signal-to-noise ratio (SNR) was calculated by the root mean square amplitude ratio of the signal and noise, and seismic records with $\text{SNR} < 2.0$ were removed. In addition, seismic events with fewer than three valid seismic records were deleted. As a result, the seismic events that were ultimately used for this study included 5181 earthquakes, with magnitudes mainly ranging from M_L 1.5 to 3.5, 5199 explosions, and 1079 mining-induced earthquakes located in the central and eastern regions of China (Fig. 1). The magnitude distribution of different seismic events is shown in Figure S1, available in the supplemental material to this article. The seismic stations are composed of China's national seismic network and regional seismic networks, most of which are broadband seismometers with a sampling rate of 100 Hz (see [Data and Resources](#)). The seismic records are mostly at local and regional distances ranging from 20 to 400 km, and the number of recording stations for seismic events is shown in Figure S1.

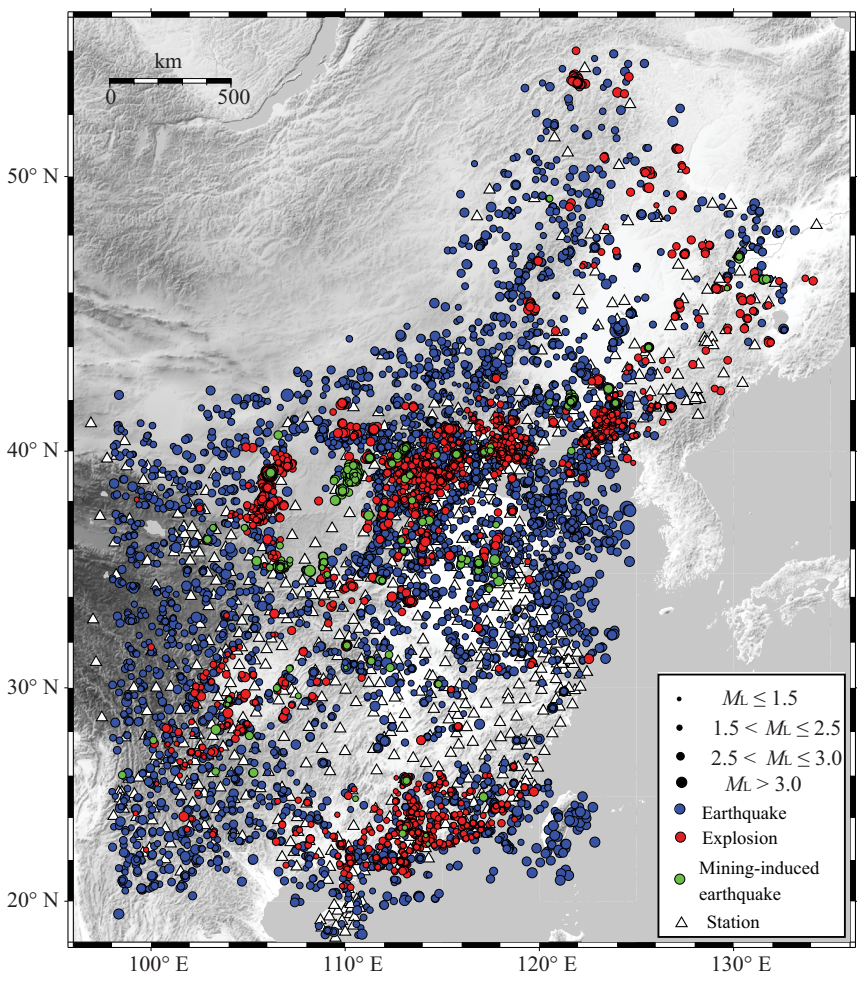


Figure 1. Locations of earthquakes (blue circles), explosions (red circles), mining-induced earthquakes (green circles), and stations (white triangles); the focal depth of the earthquakes is less than 50 km, with a magnitude between M_L 1.5 and 3.5; explosions and mining-induced earthquakes occur near the surface, with a magnitude greater than M_L 1.5.

Figure 2 compares the vertical seismic records of the three types of events. The event on 21 March 2019 was a catastrophic explosion accident at Yancheng Chemical Plant, Jiangsu Province (Fig. 2b), and the event on 21 February 2019 was a mining-induced earthquake in the Yulin mining area, Shaanxi Province (Fig. 2c). The characteristics in the seismic records are as follows: For earthquakes (Fig. 2a), the S-wave amplitude is greater than that of the P wave, and the frequencies of the P and S waves are high; explosions have larger P/S amplitude ratios than earthquakes, surface-wave development near the source, and the main frequency components of the S-wave coda and surface wave are low; mining-induced earthquakes have an unclear seismic phase distinction near the source due to the complexity of the source process, with low-frequency content and surface-wave development, and a long waveform duration; with increasing distance, the P/S amplitude ratio of these mining-induced earthquakes is larger than that of earthquakes, which is similar to explosions.

Input Parameters of AI Methods

Feature extraction dataset

Effective feature extraction methods can highlight the differences between different types of earthquakes (Pomeroy *et al.*, 1982; Douglas, 2013). Based on the preprocessed seismic records (deaveraging, detrending, and tapering), normalization by the maximum amplitude value, and filtering at 0.1–25 Hz, 36 features divided into eight categories were extracted in this article. The eight categories are as follows: amplitude ratio, high- and low-frequency energy ratio, corner frequency, waveform duration, waveform complexity, zero-crossing rate, cepstral complexity, and instantaneous frequency complexity. In Zhang *et al.* (2021), we introduced the extraction process and classification ability of these features in detail. The descriptions of these features are provided in Table 1 (more details about feature extraction are given in the supplemental material). Through feature extraction of vertical-compo-

nent seismic records from earthquakes, explosions, and mining-induced earthquakes, we constructed a 36-dimensional single-station dataset and a network-averaged dataset. The single-station dataset consists of the features of each seismic waveform, and the network-averaged dataset is obtained by arithmetically averaging the features over multiple stations for each seismic event. The distribution of the 36 features (Fig. 3), reveals that the high-frequency P/S amplitude ratios between earthquakes and explosions are more separated, and the features of mining-induced earthquakes lie between these two categories. The corner frequencies (Figs. S2 and S3), high- and low-frequency energy ratios, and zero-crossing rates of mining earthquakes are lower than those of earthquakes and explosions.

Spectral amplitude dataset

Seismic events of different types can have different spectral content. Accordingly, we also established spectral amplitude

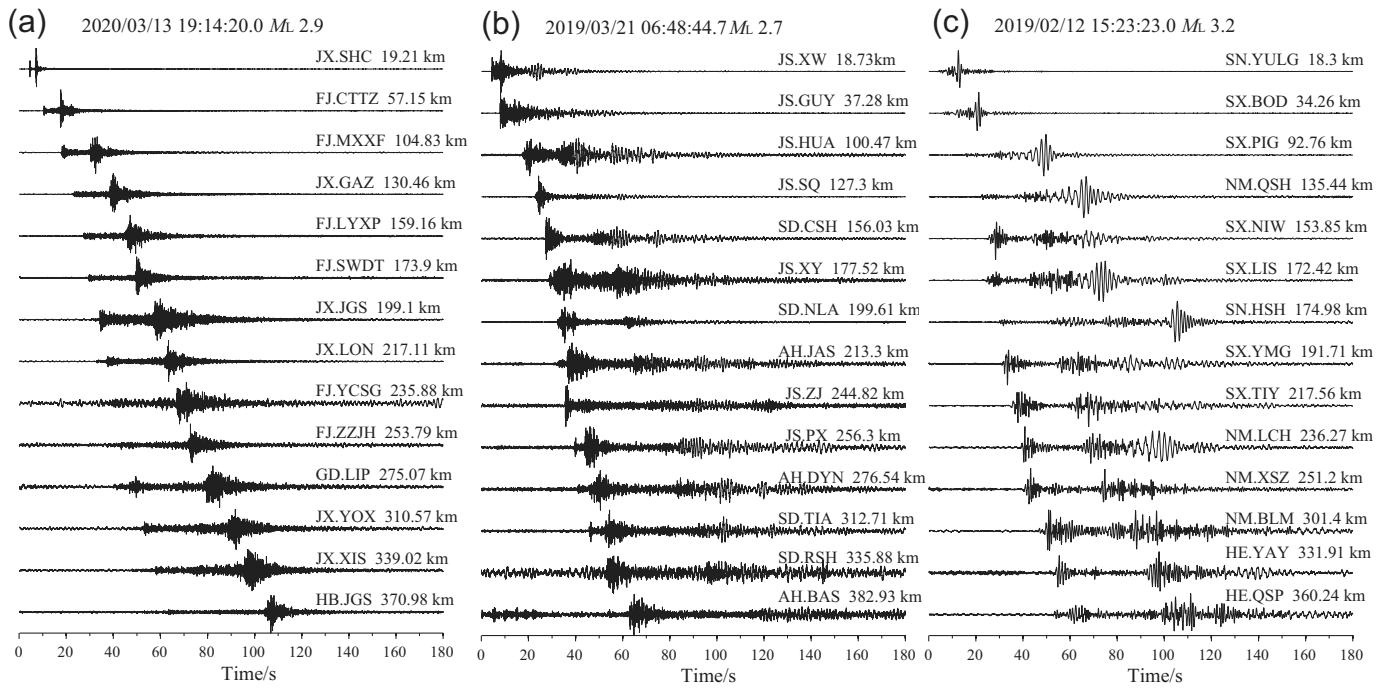


Figure 2. Waveforms of different types of events: (a) earthquake, (b) explosion, and (c) mining-induced earthquake. The occurrence time and magnitude are marked at the top of the waveform, and the station and the distance are marked at the end of

the waveform. The distances of the seismic records of different seismic events are similar, with the minimum distance of 18.3 km and the maximum distance of 382.93 km.

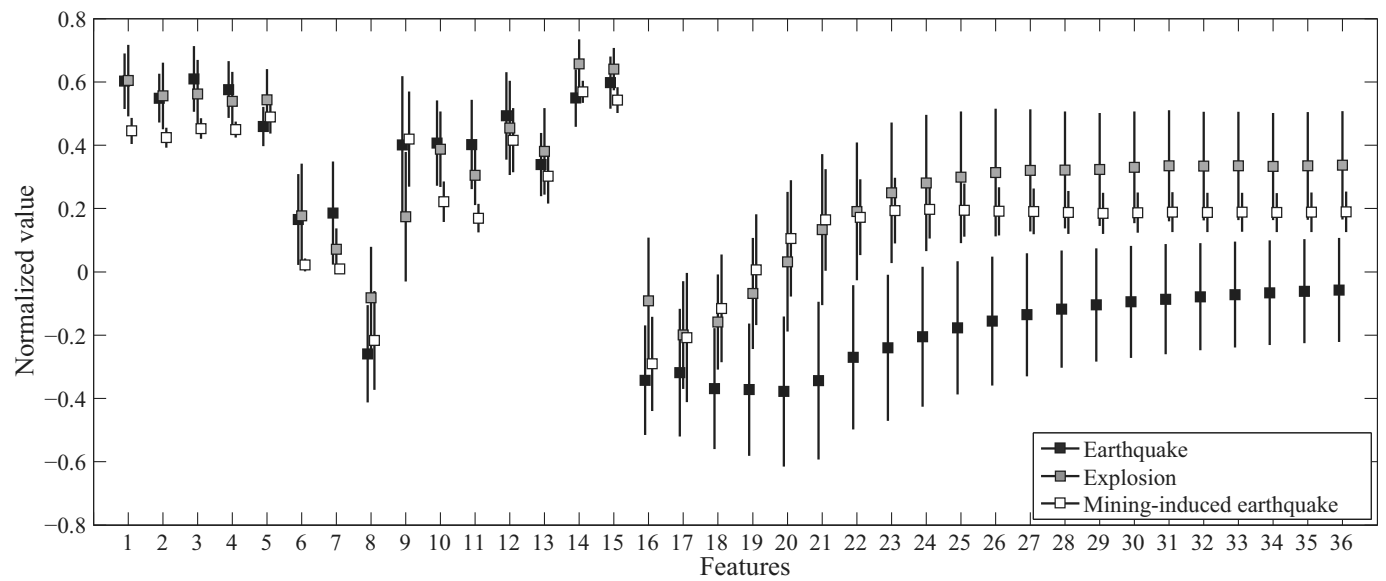


Figure 3. The average value with one standard deviation of 36 features of earthquakes (black squares), explosions (gray squares), and mining-induced earthquakes (white squares). The feature value is the maximum normalization of each feature. About 36 features are represented as follows: 1, 2: Pg corner frequency based on the source spectrum models of Brune (1970) and Jimenez et al. (2005); 3, 4: Sg corner frequency based on the

source spectrum models of Brune (1970) and Jimenez et al. (2005); 5: waveform duration; 6, 7: high- and low-frequency energy ratio of Pg and Sg ; 8, 9: waveform complexity of Pg and Sg ; 10, 11: zero-crossing rate of Pg and Sg ; 12, 13: instantaneous frequency complexity of Pg and Sg ; 14, 15: cepstral complexity of Pg and Sg ; 16: the maximum amplitude ratio of Pg/Sg ; 17–36: Pg/Sg amplitude ratios corresponding to frequencies 1–20 Hz.

TABLE 1
Input Features

Feature Type	Description	Number
Amplitude ratio	The maximum amplitude ratio of Pg/Sg is calculated, and the Pg/Sg root mean square amplitude ratios of 20 different frequency bands within 1–20 Hz after Fourier transform are also calculated as features. Wang, Bian, et al. (2021) gives the detailed calculation process for the velocity window and amplitude ratio, and the Pg/Sg amplitude ratio is the logarithmic value.	21
High- and low-frequency energy ratio	The high- and low-frequency energy ratios of Pg and Sg are extracted, in which the high-frequency band is 5–18 Hz, and the low-frequency band is 0.05–5 Hz.	2
Corner frequency	Based on the earthquake source spectrum models of Brune (1970) and Jimenez et al. (2005) , four corner frequencies of Pg and Sg are calculated as the identification features (Li et al., 2012).	4
Waveform duration	The waveform duration is defined as the ratio of the time difference between the arrival of the P -wave and the attenuation of the vibration to the noise level to the epicentral distance.	1
Waveform complexity	The energy of the explosion is concentrated mainly in the first part of the period, while the tail part is suppressed. The entire waveform is simpler than that of the earthquake (Douglas, 2013). In this article, the complexity of Pg and Sg waves is quantitatively extracted.	2
Zero-crossing rate	The zero-crossing rate is equivalent to the number of sign changes of the sampling points per second. This article quantitatively extracts the zero-crossing rate of the Pg and Sg phases.	2
Cepstral complexity	Compared with the monotonic attenuation of the explosion source, the multipeak feature of the seismic cepstrum reflects the complexity of the earthquake fault rupture in the cepstral domain (Baumgardt and Ziegler, 1988). Using the cepstral parameter extraction process in speech identification as a reference, the cepstral complexity of Pg and Sg is quantitatively extracted (Randall, 2017).	2
Instantaneous frequency complexity	Earthquakes have multiple interference phases, with instantaneous frequencies that are more complex than those of explosions. In this article, the Pg and Sg signals are subjected to the Hilbert transform to obtain the analytical signals, and then the Wigner distribution and empirical mode decomposition are used to obtain the instantaneous frequency. Finally, the instantaneous frequency complexity of Pg and Sg is quantitatively extracted as the criterion.	2

datasets of vertical-component seismic records. Unlike feature extraction, the calculation process is simple. First, we used a theoretical velocity window to select the full waveform including P and S signals. Second, for all seismic records, basic processing (deaveraging, detrending, and tapering) was performed, and the results were normalized by the maximum amplitude value and filtered at 0.1–25 Hz. Third, the Thomson multitaper spectrum estimation method ([Thomson, 1982, 2007](#)) was used to calculate the spectral amplitude for each seismic record (more details about the theoretical velocity window and the calculation formula are given in the supplemental material), in which 512 points were used for fast Fourier transform, and the frequency resolution was 100/512 Hz. Figure 4 shows the network-averaged spectral amplitude between 0 and 25 Hz of earthquakes, explosions, and mining-induced earthquakes. We uniformly extracted 60 amplitude spectra from the frequency logarithmically (log 2) discrete distribution as a 60-dimensional spectral amplitude dataset, including single-station and network-averaged datasets.

Input parameters

The feature extraction and spectral amplitude datasets were used as the input parameters for the five AI methods. Earthquakes

were labeled 0, explosions were labeled 1, and mining-induced earthquakes were labeled 2. We separated 801 earthquakes, 846 explosions, and 247 mining-induced earthquakes that have occurred in the recent years as a test dataset to evaluate the generalizability of the classification model, and the remaining data were used for training and validation. The number of training and test datasets is shown in Table 2.

AI Methods

SVM

SVMs are supervised learning algorithms based on statistical learning theory and the principle of structural risk minimization ([Cortes and Vapnik, 1995; Vapnik, 1995](#)). SVMs have a simple structure and good generalization ability, and are effective in high-dimensional spaces ([Kortström et al., 2016](#)). The kernel function can solve complex problems, map training data to high-dimensional spaces, and calculate the largest classification hyperplane between classes in high-dimensional spaces ([Samui, 2008](#)). Before the advent of deep learning, SVM became a popular algorithm in machine learning, that is, SVMs were considered to perform well, and were widely used in data analysis and event classification ([Devos et al., 2014; Tang et al., 2020](#)).

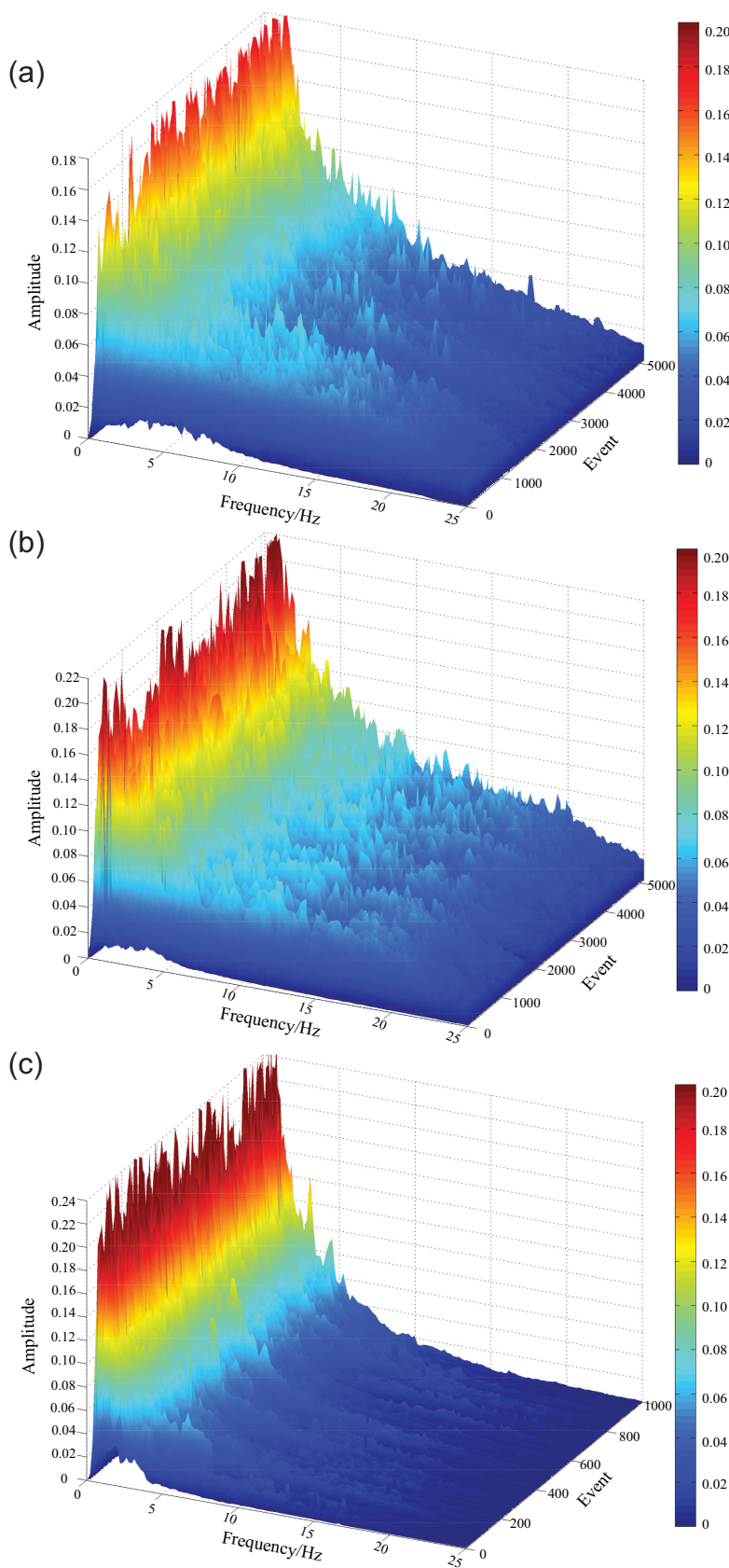


Figure 4. Network-averaged spectral amplitude distribution of (a) 5181 earthquakes, (b) 5199 explosions, and (c) 1079 mining-induced earthquakes.

XGBoost

XGBoost is a flexible and portable recently developed boosting decision tree algorithm proposed by [Chen and Guestrin \(2016\)](#). The XGBoost algorithm performs a second-order Taylor expansion on the loss function and adds a regularization term, thereby effectively preventing overfitting and increasing the convergence speed ([Parsa et al., 2020](#)). By continuously forming new decision trees to fit the residuals of the previous predictions, the residuals between the predicted and actual values are continuously reduced, thereby improving the prediction accuracy. XGBoost is one of the most widely used machine learning algorithms in the field of data science ([Nguyen et al., 2019](#); [Wang, Yu, et al., 2021](#)), although it has been less commonly applied in seismology research.

LSTM networks

[Hochreiter and Schmidhuber \(1997\)](#) proposed an LSTM network to address the vanishing gradient problem in recurrent neural networks (RNNs). An LSTM network consists of a storage unit, an input gate, a forget gate, and an output gate ([Kumar et al., 2019](#)). LSTM networks are mainly used to deal with time series problems. LSTM networks perform layer-by-layer learning on the input sequence data and adaptively extract features, thereby preventing the need to select and extract features manually. The softmax function is used to classify the output results. Good results have been achieved in speech recognition, signal recognition, and seismic event discrimination ([Linville et al., 2018](#)).

TABLE 2
The Number of Training and Test Datasets

Label	Number of Training Datasets		Number of Test Datasets	
	Network Averaged	Single Station	Network Averaged	Single Station
0	4380	116938	801	18614
1	4353	99359	846	11624
2	832	33787	247	11036

Labels: 0, earthquakes; 1, explosions; and 2, mining-induced earthquakes.

2019; Woellmer *et al.*, 2013; Naresh and Duraipandian, 2021; Zhou *et al.*, 2021).

ResNet

Deeper networks can better fit more complex problems, He *et al.* (2016) found that when simply stacked layers are used to fit complex features, the network is prone to degradation when it is too deep; therefore, residuals are introduced into the neural network. Residuals can solve the gradient dispersion and accuracy decline in deep networks, reduce information loss, and improve the convergence speed of the network (Szegedy *et al.*, 2016). ResNet has been applied in handwriting recognition, speech recognition, and seismic event classification (Habibzadeh *et al.*, 2018; Wei *et al.*, 2019).

LSTM-FCN

LSTM can learn the time dependence in a sequence but has difficulty working with long-term dependence in a sequence. Karim *et al.* (2017, 2019) proposed the LSTM-FCN model by combining LSTM and fully convolutional networks (FCNs, Long *et al.*, 2015). The LSTM-FCN simultaneously extracts the local features and long-term dependence of the time series, and has been widely used in gesture recognition and data enhancement (Tang *et al.*, 2021; Wang, Liu, *et al.*, 2021).

Analysis of Results and Discussion

Based on 36-dimensional feature extraction datasets and 60-dimensional spectral amplitude datasets, we established two-class and three-class models to classify earthquakes, explosions, and mining-induced earthquakes through five AI methods (SVM, XGBoost, LSTM, ResNet, and LSTM-FCN). The GridSearchCV function in scikit-learn of Python 3.8 software was used to optimize the main parameters of SVM and XGBoost. LSTM, ResNet, and LSTM-FCN, relying on the Keras interface to TensorFlow, were used for building and training the classifiers (more details about the optimization of the hyperparameters are given in Fig. S4).

Generally, undersampling and upsampling are used to address the problem of data imbalance (Um *et al.*, 2017;

Miao *et al.*, 2020; Parsa *et al.*, 2020). In this work, we compared the undersampling and data augmentation methods (more details about the comparison between data augmentation and undersampling are given in Fig. S5) and finally adopted the undersampling method to address the data imbalance, that is, we randomly sampled smaller amount of data from classes with more samples, so the amount of data selected was reduced to the same amount of data that was sampled from classes with fewer samples. To verify the model performance, we employed a fivefold cross validation (Kohavi, 1995). The training dataset was randomly divided into five subsamples, and the training of the model was conducted on four subsets, while the validation was performed by the remaining subset. The training and validating process was repeated five times, with different subsets being used as the validating set. To test the stability of the five AI methods, we conducted fivefold cross validation 10 times for each classifier, randomly resampling the training data at every run, with a total of 50 validation results.

To compare the model performance of different AI methods, the same datasets were used in each cross validation. Accuracy, true negative rate (TNR), true positive rate (TPR), receiver operating characteristic (ROC), area under ROC curve (AUC), and F1-Score were used to evaluate the performance of different classifiers (more details about the definition of performance measures are given in the supplemental material).

Classification results of the network-averaged datasets

We analyzed the importance of features through XGBoost and random forest (RF) algorithm. Gini importance, which is a measure of variable importance based on the Gini impurity index, with variable importance scores normalized (the sum of all importance scores is 1) (Qi, Fourie, Du, *et al.*, 2018; Song *et al.*, 2020). The P/S amplitude ratio has long played an important role in earthquake/explosion classification; the importance of 36 features calculated by XGBoost and RF differs slightly (Joharestani *et al.*, 2019; AlThuwaynee *et al.*, 2021), but the high-frequency P/S amplitude ratios all ranked higher. By selecting the number of features through importance, a higher accuracy can be obtained by selecting 16 to all features (more details about the feature importance and feature selection are given in Fig. S6). In this study, we did not conduct more feature analysis and selection, but input all features.

Figure 5 shows the accuracies and ROC curves of different AI models, revealing that the accuracies of the five AI models on the 36-dimensional feature extraction dataset are approximately 14%, 7%, and 2% greater than those on the 60-dimensional spectral amplitude dataset in the classification of 0-1, 0-2, and 1-2, respectively. These findings indicated that the feature extraction method used in this article can more effectively highlight the differences among earthquakes, explosions, and mining-induced earthquakes.

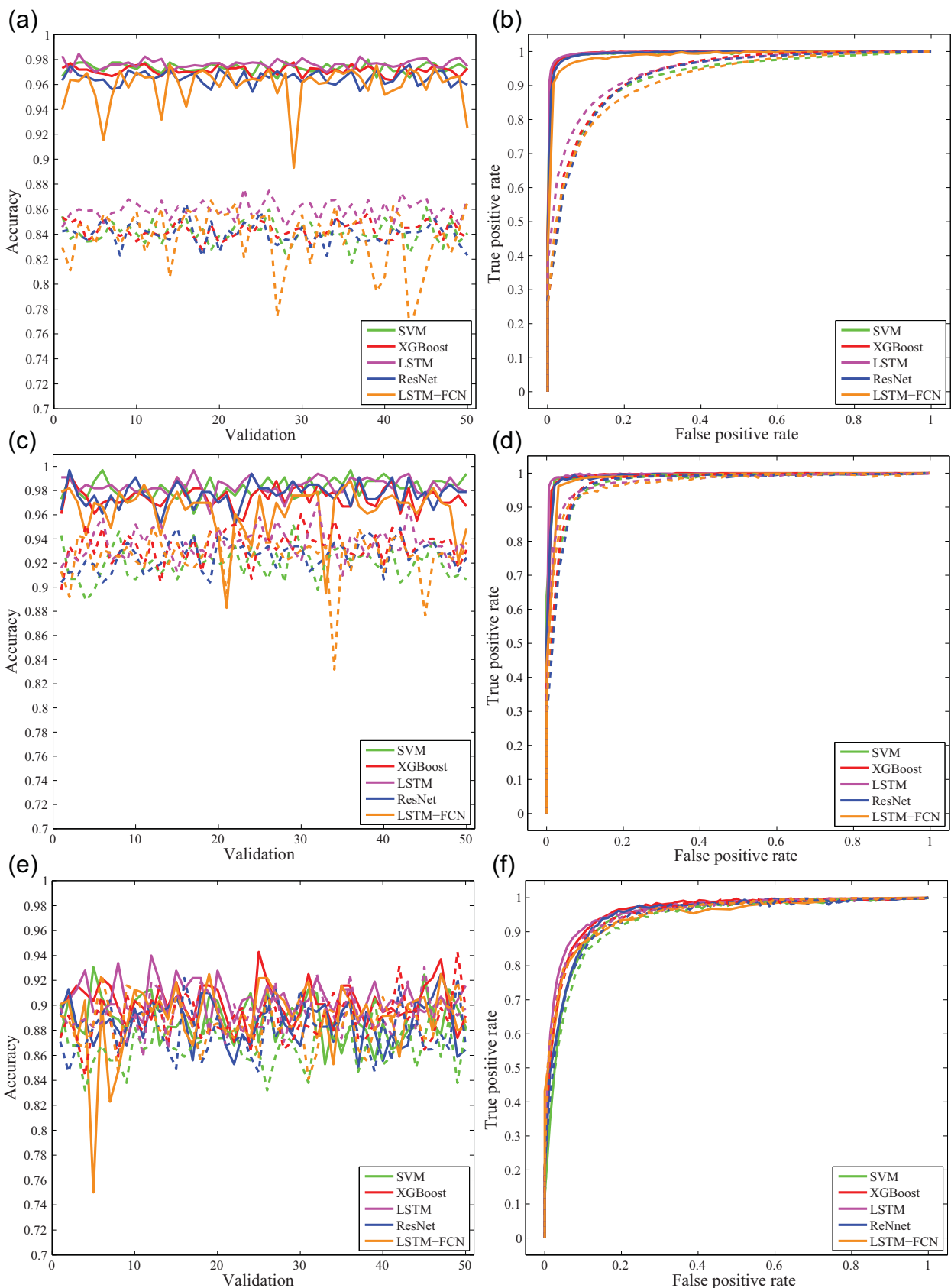


Figure 5. The accuracies obtained on 50 validations and receiver operating characteristic (ROC) curves by different artificial intelligence (AI) methods on the network-averaged dataset in (a) 0-1, (c) 0-2, and (e) 1-2 classification; ROC curves for (b) 0-1,

(d) 0-2, and (f) 1-2 classification. The solid and dashed lines indicate the 36-dimensional and 60-dimensional datasets, respectively. Earthquakes, explosions, and mining-induced earthquakes are labeled 0, 1, and 2, respectively.

TABLE 3

Validation Accuracies of Three-Class Artificial Intelligence (AI) Models for Earthquakes, Explosions, and Mining-Induced Earthquakes

AI Methods	Network-Averaged Dataset						Single-Station Dataset					
	36 Dimensional			60 Dimensional			36 Dimensional			60 Dimensional		
	0	1	2	0	1	2	0	1	2	0	1	2
SVM	0.962	0.828	0.913	0.789	0.675	0.820	-	-	-	-	-	-
XGBoost	0.936	0.854	0.912	0.779	0.747	0.893	0.868	0.754	0.844	0.703	0.629	0.818
LSTM	0.960	0.861	0.916	0.783	0.703	0.876	0.880	0.707	0.821	0.750	0.558	0.778
ResNet	0.931	0.846	0.885	0.760	0.723	0.841	0.866	0.709	0.811	0.724	0.595	0.761
LSTM-FCN	0.941	0.817	0.883	0.796	0.700	0.857	0.861	0.670	0.725	0.731	0.533	0.7483

Labels: 0, earthquakes; 1, explosions; and 2, mining-induced earthquakes. LSTM, long short-term memory network; LSTM-FNC, long short-term memory fully convolutional network; ResNet, residual neural network; SVM, support vector machine; and XGBoost, extreme gradient boosting.

The performance of the different AI models in 0-2 classification was the greatest, with average accuracies from 97.4% to 98.4%; the next greatest accuracy was in 0-1 classification, with average accuracies from 96.5% to 97.6%; and the average accuracies in 1-2 were from 88.8% to 90.6%. Table S2 shows the average TPR and TNR results of two-class models on network-averaged datasets. In the three-class, the accuracies achieved by different AI models were the greatest for earthquakes, followed by mining-induced earthquakes and explosions. The average accuracies of the LSTM on the 36-dimensional dataset were 96% for earthquakes, 91.6% for mining-induced earthquakes, and 86.1% for explosions (Table 3).

In terms of machine learning, the larger the AUC value is the better the classifier (Qi, Fourie, Ma, et al., 2018; Binh et al., 2020). SVM, XGBoost, LSTM, and ResNet obtained stable and high accuracies on the network-averaged dataset, with AUC values all greater than 0.9 (Table S4), indicating that these methods are suitable for the data structure used in this article. For the LSTM-FCN model, after parameter adjustment processes similar to those used in other models, the accuracy nonetheless remained unstable.

Classification results of single-station datasets

The single-station dataset has a relatively large amount of data (Table 2). Most machine learning algorithms and pattern recognition methods, such as SVM and Fisher, are not suitable for large datasets (Chau et al., 2014). Figure 6 shows the accuracies and ROC curves by other four AI models (XGBoost, LSTM, ResNet, and LSTM-FCN) on the single-station dataset.

1. The performance on single-station and network-averaged datasets showed similar results; that is, the accuracies based on the 36-dimensional feature extraction dataset in 0-1 and 0-2 classification increased by approximately 15% and 6%,

respectively, compared to those of the 60-dimensional spectral amplitude dataset, indicating that effective feature extraction can highlight the differences between different seismic events. In contrast, the accuracy when classifying 1-2 was lower, because both explosions and mining-induced earthquakes occur near the surface. The feature extraction method in this article cannot fully highlight the differences, and more feature extraction methods that can highlight differences between these two types of shallow seismic events need to be explored.

2. The performance of the different AI models with single-station datasets in the 0-2 classification was the greatest, with accuracies from 92.63% to 94.32%; the next greatest performance was found in 0-1 classification, with accuracies from 90.27% to 92.17%, whereas the performance when classifying 1-2 was relatively weak, with accuracies from 82.07% to 82.93%. Table S3 shows the average TPR and TNR results of two-class models on single-station datasets. In the three-class on the 36-dimensional dataset, XGBoost performed the best, with an average accuracy of 86.8% for earthquakes, 75.4% for explosions, and 84.4% for mining-induced earthquakes (Table 3).
3. The network-averaged P/S spectral ratios can provide much better discrimination power than single-station P/S spectral ratios (Kim et al., 1997, 2018; O'Rourke et al., 2016). Our study showed that the accuracies obtained with the single-station dataset were, approximately, 5%, 6%, and 8% less than those obtained with the network-averaged dataset in 0-2, 0-1, and 1-2 discrimination, respectively. Therefore, the network-averaged datasets are recommended to classify unnatural seismic events.
4. In the two-class and three-class classifications of earthquakes, explosions and mining earthquakes with single-station dataset by four AI methods, XGBoost, and LSTM had better performance, higher accuracy, and AUC value (Table S4).

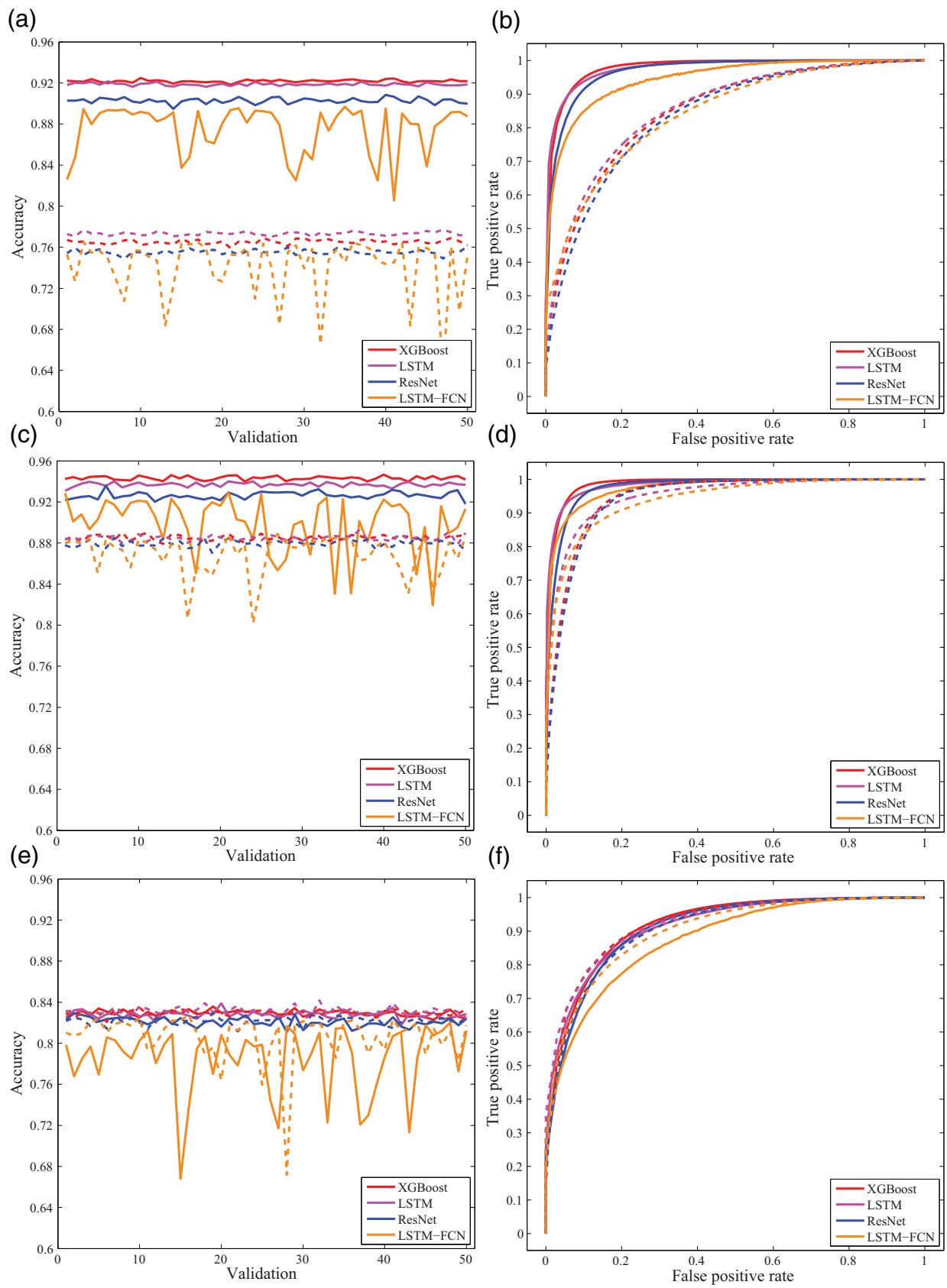


Figure 6. The accuracies obtained on 50 validations and ROC curves by different AI methods on the single-station dataset in (a) 0-1, (c) 0-2, and (e) 1-2 classification; ROC curves for (b) 0-1, (d) 0-2, (f) and 1-2 classification. The solid and dashed lines

indicate the 36-dimensional and 60-dimensional datasets, respectively. Earthquakes, explosions, and mining-induced earthquakes are labeled 0, 1, and 2, respectively.

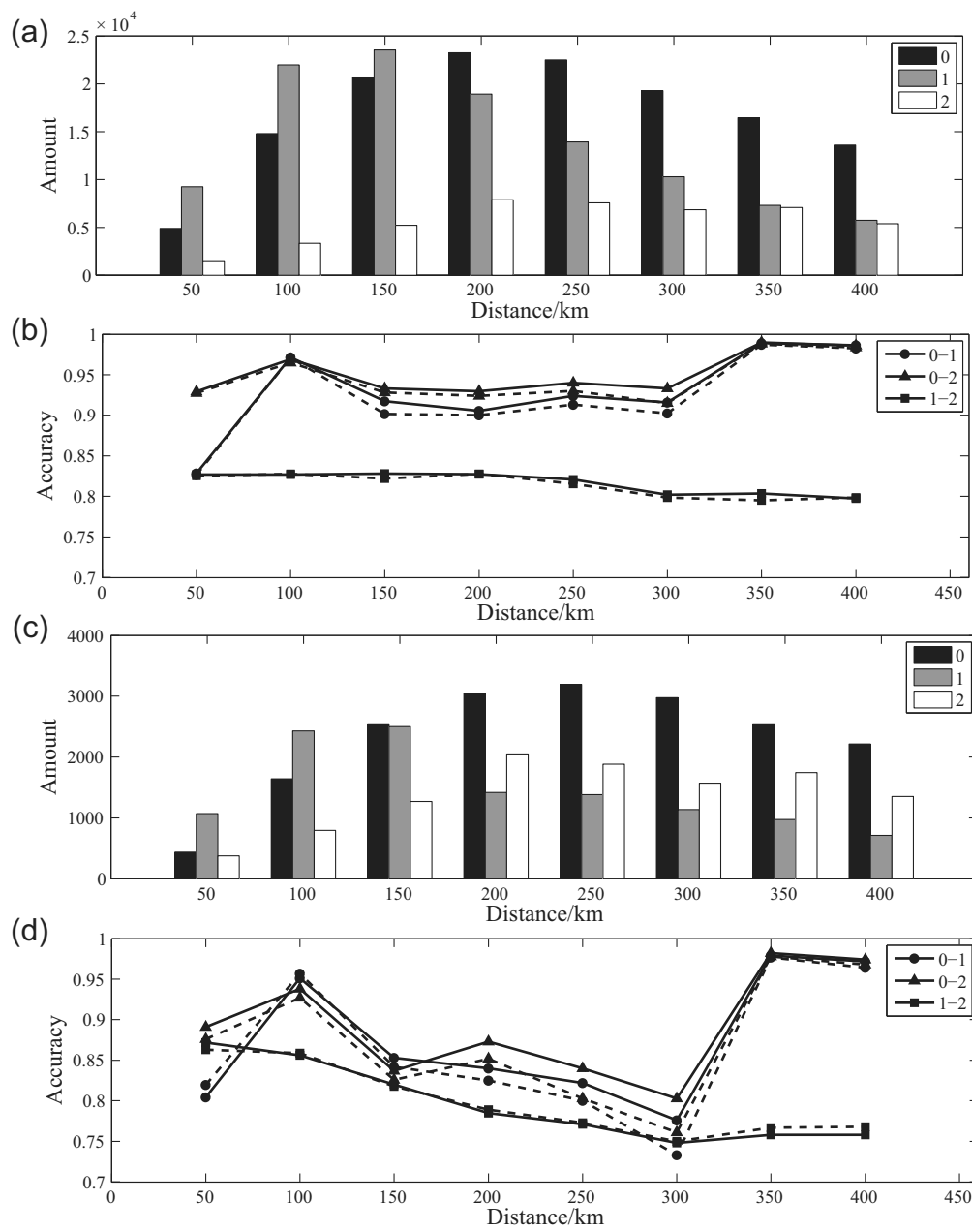


Figure 7. (a) Numbers and (b) accuracies on the 36-dimensional training dataset with different epicentral distances; (c) numbers and (d) accuracies on the 36-dimensional test dataset with different epicentral distances. The solid line and the dashed line indicate extreme gradient boosting (XGBoost) and long short-term memory network (LSTM) methods, respectively. Earthquakes, explosions, and mining-induced earthquakes are labeled 0, 1, and 2, respectively.

Variation in classification accuracy with epicentral distance

Pyle and Walter (2019) concluded that the P/S discriminant in earthquakes/explosions classification performed more poorly for distances less than 100 km and failed at distances less than 50 km, which is possibly because of the mixing of Rg in the Lg measurement or the generation of shear waves near the source (Pitarka *et al.*, 2015; O'Rourke *et al.*, 2016; Wang, Bian, *et al.*, 2021). In this article, the single-station dataset was segmented at

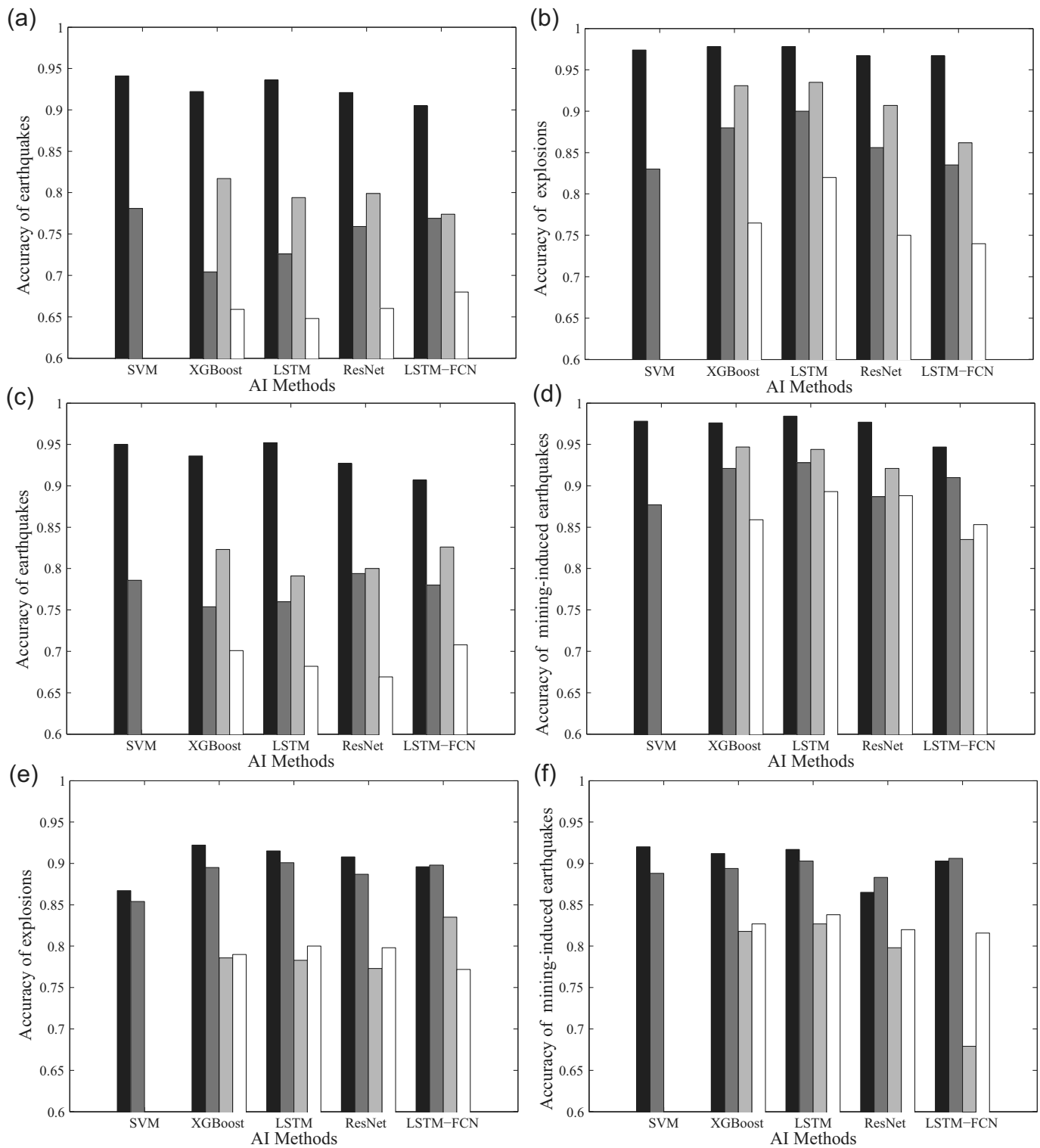
an interval of 50 km to analyze the variation in the accuracies. The different AI models used in the previous comparison show that XGBoost, LSTM, and ResNet can all achieve stable classification ability based on the single training set. In this work, we used XGBoost and LSTM to construct different classifiers to study the change of accuracy with epicentral distance (Fig. 7) and get that the trend of the accuracy change with the epicentral distance is similar on the 36-dimensional training set and the test set.

For 0-1 classification, the test accuracy was less than 82% within 50 km. For 0-1 and 0-2 classification, the test accuracies were enhanced at 50–100 km, reaching 93%. These values were reduced within 100–300 km and then increased again at distances greater than 300 km. This may be related to the rapid attenuation of high-frequency signals of unnatural seismic events and the low SNR of high-frequency at distances greater than 300 km. Figure S7 shows the variation in the SNR with epicentral distance and frequency. Although seismic records with $SNR > 2.0$ exist in the time domain above 300 km, the high-frequency energy in the signal is missing, and the SNR of high frequencies is low, especially for mining-induced earthquakes.

Increasing with epicentral distance, the accuracy in 0-1 and 0-2 classification exhibited similar trends, and the accuracy in 1-2 discrimination decreased gradually, indicating that the seismic records of explosions and mining-induced earthquakes are similar not only at nearby but also at greater distances.

Assessment of the generalizability of the event classifier

To evaluate the generalizability of the classifiers, it can be seen in Figure 8 and Table S5 that the test accuracies and



F1-Scores of the two-class models with the 36-dimensional network-averaged test dataset both exceed 90%, of which F1-Score ranges of the 0-1 classifier, 0-2 classifier, and 1-2 classifier are 93.7%–95.8%, 92%–96.1%, and 90.1%–92.2%, respectively. The test accuracies on the 36-dimensional network-averaged and single-station datasets were higher than those of the 60-dimensional datasets, and the test accuracies of network-averaged datasets were higher than those of the

Figure 8. Test accuracies of two-class models achieved by different AI methods, (a) and (b) are the 0-1 classifier, (c) and (d) are the 0-2 classifier, (e) and (f) are the 1-2 classifier. The black, dark gray, light gray, and white represent 36-dimensional network-averaged dataset, 60-dimensional network-averaged dataset, 36-dimensional single-station dataset, and 60-dimensional single-station dataset, respectively.

TABLE 4

Test Accuracies of Three-Class AI Models for Earthquakes, Explosions, and Mining-Induced Earthquakes

AI Methods	Network-Averaged Dataset						Single-Station Dataset					
	36 Dimensional			60 Dimensional			36 Dimensional			60 Dimensional		
	0	1	2	0	1	2	0	1	2	0	1	2
SVM	0.914	0.832	0.906	0.659	0.691	0.767	—	—	—	—	—	—
XGBoost	0.852	0.902	0.902	0.555	0.809	0.870	0.732	0.736	0.811	0.523	0.630	0.793
LSTM	0.899	0.900	0.909	0.607	0.769	0.867	0.757	0.703	0.778	0.603	0.574	0.764
ResNet	0.820	0.877	0.860	0.625	0.769	0.797	0.736	0.694	0.776	0.589	0.603	0.737
LSTM-FCN	0.845	0.864	0.855	0.669	0.740	0.852	0.733	0.666	0.689	0.612	0.570	0.736

Labels: 0, earthquakes; 1, explosions; and 2, mining-induced earthquakes. LSTM, long short-term memory network; LSTM-FNC, long short-term memory fully convolutional network; ResNet, residual neural network; SVM, support vector machine; and XGBoost, extreme gradient boosting.

single-station datasets, which are consistent with the training results. In the comparison of the five AI methods, XGBoost and LSTM had higher test accuracies than the other methods.

Among the three-class models tests (Table 4), LSTM with 36-dimensional network-averaged dataset had the best performance, with test accuracies of 89.9% for earthquakes, 90% for explosions, and 90.9% for mining-induced earthquakes. The generalizability of three-class models with other datasets was relatively weak. The test results showed that the two-class and three-class models of XGBoost and LSTM had high test accuracies, high F1-Scores, and a strong generalizability on the 36-dimensional feature extraction dataset. We recommend that these approaches be given priority in practical applications.

Conclusion

This article establishes training and test dataset through feature extraction and multiwindow spectral analysis; it uses five AI methods to classify different seismic events, that is, earthquakes, explosions, and mining-induced earthquakes, and obtains the following conclusions:

1. The accuracies obtained with the network-averaged dataset are greater than those obtained with the single-station dataset. Based on the network-averaged dataset, the performance of different AI models in 0-2 classification was the greatest, with average accuracies from 97.4% to 98.4%; the average accuracies in 0-1 classification were from 96.5% to 97.6%; and the average accuracies in 1-2 were from 88.8% to 90.6%.
2. With both the network-averaged and single-station datasets, the accuracies obtained on the 36-dimensional feature extraction dataset were greater than those of 60-dimensional spectral amplitude dataset, indicating that the feature extraction methods used in this article can effectively highlight the differences in the seismic records of different types of events.

3. SVM, XGBoost, LSTM, and ResNet all performed well in the classification on network-averaged dataset, with AUC values all greater than 0.9. In the classification with single-station dataset, XGBoost and LSTM had better performance and higher accuracy, indicating that these models have good application prospects for seismic event classification.

4. In the model generalization evaluation, the test accuracies and F1-Scores of the two-class models with the 36-dimensional network-averaged dataset both exceeded 90%. The test accuracies of the three-class model by LSTM were 89.9% for earthquakes, 90% for explosions, and 90.9% for mining-induced earthquakes. The test results showed that the two-class and three-class models of XGBoost and LSTM have high test accuracies, high F1-Scores, and a strong generalizability with the 36-dimensional feature extraction dataset and are preferred in practical applications.

In the future work, we will continue to expand the types of seismic events, including rockslides, landslides, and induced earthquakes, and carry out additional extraction methods. We will further collect unnatural seismic events in more regions of China to popularize and verify the trained AI models, and continue to improve the accuracy of AI methods through data preprocessing, feature selection, and algorithm integration.

Data and Resources

The seismic catalogs were obtained through the earthquake cataloging system available at <http://10.5.160.18/console/index.action> (last accessed September 2022, the access should be obtained from the Institute of Geophysics, China Earthquake Administration), the Beijing Digital Seismic Network, and Earthquake monitoring centers of Liaoning, Shaanxi, Shanxi, and Guangdong Provinces, China. The seismic data used in this study were obtained from the Data Management Centre of China National Seismic Network (SEISDMC; <http://www.esdc.ac.cn>, last accessed November 2022) at the Institute of Geophysics, China Earthquake Administration. The Keras (<https://keras.io>, last accessed September 2022) interface to TensorFlow

(<https://github.com/tensorflow>, last accessed September 2022) was used for building and training the artificial neural networks (long short-term memory network [LSTM], residual network [RESNET] and long short-term memory fully convolutional network [LSTM-FCN]). The Python Sklearn (<https://scikit-learn.org/stable>, last accessed September 2022) and extreme gradient boosting (XGBoost; <https://xgboost.ai>, last accessed September 2022) packages were used for support vector machine (SVM) and XGBoost. The map was made using Generic Mapping Tools (<https://www.soest.hawaii.edu/gmt>, last accessed February 2022). The supplemental material includes details on feature extraction and spectral amplitude dataset, the optimization of hyperparameters, the definition of performance measures, comparison between data augmentation and undersampling, and feature importance and feature selection.

Declaration of Competing Interests

The authors acknowledge that there are no conflicts of interest recorded.

Acknowledgments

The authors are grateful for the comments from the editor, the guest editor, and the three anonymous reviewers that helped to improve this article. The authors would like to thank the Data Management Centre of China National Seismic Network at the Institute of Geophysics, China Earthquake Administration for providing the seismic data for this study. Our work was supported by the Special Fund of the Institute of Geophysics, China Earthquake Administration (JY2022Z36).

References

- AlThuwaynee, O. F., S. W. Kim, M. A. Najemaden, A. Aydda, A. L. Balogun, M. M. Fayyadh, and H. J. Park (2021). Demystifying uncertainty in PM10 susceptibility mapping using variable drop-off in extreme-gradient boosting (XGB) and random forest (RF) algorithms, *Environ. Sci. Pollut. Res.* doi: [10.1007/s11356-021-13255-4](https://doi.org/10.1007/s11356-021-13255-4).
- Baumgardt, D. R., and K. A. Ziegler (1988). Spectral evidence for source multiplicity in explosions: Application to regional discrimination of earthquakes and explosion, *Bull. Seismol. Soc. Am.* **78**, 1173–11795, doi: [10.1016/0040-1951\(88\)90003-0](https://doi.org/10.1016/0040-1951(88)90003-0).
- Binh, T. P., N. Trung, Q. Chong, V. P. Tran, D. Jie, S. H. Lanh, V. L. Hiep, and P. Indra (2020). Coupling RBF neural network with ensemble learning techniques for landslide susceptibility mapping, *Catena* **195**, 104,805, doi: [10.1016/j.catena.2020.104805](https://doi.org/10.1016/j.catena.2020.104805).
- Brune, J. N. (1970). Tectonic stress and the spectra of seismic shear wave from earthquake, *J. Geophys. Res.* **75**, 4997–5009, doi: [10.1029/jb075i026p04997](https://doi.org/10.1029/jb075i026p04997).
- Chau, A. L., X. Li, and W. Yu (2014). Support vector machine classification for large datasets using decision tree and Fisher linear discriminant, *Future. Generat. Comput. Syst.* **36**, 57–65, doi: [10.1016/j.future.2013.06.021](https://doi.org/10.1016/j.future.2013.06.021).
- Chen, T. Q., and C. Guestrin (2016). XGBoost: A scalable tree boosting system, *Proc. of the 22nd ACM SIGKDD International Conf. on Knowledge Discovery and Data Mining*, San Francisco, 785–794, doi: [10.1145/2939672.2939785](https://doi.org/10.1145/2939672.2939785).
- Cortes, C., and V. Vapnik (1995). Support-vector networks, *Mach. Learn.* **20**, 273–297, doi: [10.1023/A:1022627411411](https://doi.org/10.1023/A:1022627411411)
- Devos, O., G. Downey, and L. Duponchel (2014). Simultaneous data pre-processing and SVM classification model selection based on a parallel genetic algorithm applied to spectroscopic data of olive oils, *Food. Chem.* **148**, 124–130, doi: [10.1016/j.foodchem.2013.10.020](https://doi.org/10.1016/j.foodchem.2013.10.020).
- Douglas, A. (2013). *Forensic Seismology and Nuclear Test Bans*, Cambridge University Press, 342–344, doi: [10.1017/CBO9781139524001](https://doi.org/10.1017/CBO9781139524001).
- Fisk, M. D., S. R. Taylor, W. R. Walter, and G. E. Randall (2009). Seismic event discrimination using two-dimensional grids of regional P/S spectral ratios applications to Novaya Zemlya and The Korea peninsula, *Proc. of the 2009 Monitoring Research Review*, Tucson, Arizona, 21–23 September 2009, 465–474.
- Ford, S. R., D. S. Dreger, and W. R. Walter (2009). Source analysis of the Memorial Day explosion, Kimchaek, North Korea, *Geophys. Res. Lett.* **12**, 15,644, doi: [10.1029/2009gl040003](https://doi.org/10.1029/2009gl040003).
- Habibzadeh, M., M. Jannesari, Z. Rezaei, H. Baharvand, and M. Totonchi (2018). Automatic white blood cell classification using pre-trained deep learning models: ResNet and inception, *Proc. SPIE* **10696**, 1069612, doi: [10.1117/12.2311282](https://doi.org/10.1117/12.2311282).
- He, K., X. Zhang, S. Ren, and J. Sun (2016). Deep residual learning for image recognition, *Proc. of the IEEE Conf. on Computer Vision and Pattern Recognition*, 770–778.
- Hochreiter, S., and J. Schmidhuber (1997). Long short-term memory, *Neural. Comput.* **9**, 1735–1780, doi: [10.1162/neco.1997.9.8.1735](https://doi.org/10.1162/neco.1997.9.8.1735).
- Holt, M. M., K. D. Koper, W. Yeck, S. D'Amico, Z. Li, J. M. Hale, and R. Burlacu (2019). On the portability of ML-Mc as a depth discriminant for small seismic events recorded at local distances, *Bull. Seismol. Soc. Am.* **109**, 1661–1673, doi: [10.1785/0120190096](https://doi.org/10.1785/0120190096).
- Jimenez, A., J. M. Garcia, and M. D. Romacho (2005). Simultaneous inversion of source parameters and attenuation factor using genetic algorithms, *Bull. Seismol. Soc. Am.* **95**, 1401–1411, doi: [10.1785/0120040116](https://doi.org/10.1785/0120040116).
- Joharestani, M. Z., C. Cao, X. Ni, B. Bashir, and S. Talebiesfandarani (2019). PM2.5 prediction based on random forest, XGBoost, and deep learning using multisource remote sensing data, *Atmosphere* **10**, 373, doi: [10.3390/atmos10070373](https://doi.org/10.3390/atmos10070373).
- Karim, F., S. Majumdar, and H. Darabi (2019). Insights into LSTM fully convolutional networks for time series classification, *IEEE Access* **7**, 67,718–67,725, doi: [10.1109/access.2019.2916828](https://doi.org/10.1109/access.2019.2916828).
- Karim, F., S. Majumdar, H. Darabi, and S. Chen (2017). LSTM fully convolutional networks for time series classification, *IEEE Access* **6**, 1662–1669, doi: [10.1109/ACCESS.2017.2779939](https://doi.org/10.1109/ACCESS.2017.2779939).
- Kim, W. Y., V. Aharonian, A. Lernerlam, and P. G. Richards (1997). Discrimination of earthquakes and explosions in southern Russia using regional high-frequency three-component data from the IRIS/JSP Caucasus network, *Bull. Seismol. Soc. Am.* **87**, 569–588, doi: [10.1785/BSSA0870030569](https://doi.org/10.1785/BSSA0870030569).
- Kim, W. Y., P. G. Richards, D. P. Schaff, E. Jo, and Y. Ryoo (2018). Identification of seismic events on and near the North Korean test site after the underground nuclear test explosion of 3 September 2017, *Seismol. Res. Lett.* **89**, 2120–2130, doi: [10.1785/0220180133](https://doi.org/10.1785/0220180133).
- Kohavi, R. (1995). A study of cross-validation and bootstrap for accuracy estimation and model selection, *Proc. of the International Joint Conf. on Artificial Intelligence*, Morgan Kaufmann Publishers Inc, Stanford University, 895–900.
- Koper, K. D., J. C. Pechmann, R. Burlacu, K. L. Pankow, J. Stein, J. M. Hale, P. Roberson, and M. K. McCarter (2016). Magnitude-based discrimination of man-made seismic events from naturally

- occurring earthquakes in Utah, USA, *Geophys. Res. Lett.* **43**, 10,638–10,645, doi: [10.1002/2016gl070742](https://doi.org/10.1002/2016gl070742).
- Kortström, J., M. Uski, and T. Tiira (2016). Automatic classification of seismic events within a regional seismograph network, *Comput. Geosci.* **87**, 22–30, doi: [10.1016/j.cageo.2015.11.006](https://doi.org/10.1016/j.cageo.2015.11.006).
- Kumar, S., A. Sharma, and T. Tsuno Da (2019). Brain wave classification using long short-term memory network based OPTICAL predictor, *Sci. Rep.* **9**, 9153, doi: [10.1038/s41598-019-45605-1](https://doi.org/10.1038/s41598-019-45605-1).
- Kuyuk, H. S., E. Yildirim, E. Dogan, and G. Horasan (2012). Application of k-means and Gaussian mixture model for classification of seismic activities in Istanbul, *Nonlinear. Process. Geophys.* **19**, 411–419, doi: [10.5194/npg-19-411-2012](https://doi.org/10.5194/npg-19-411-2012).
- Kuyuk, H. S., E. Yildirim, E. Dogan, and G. Horasan (2014). Clustering seismic activities using linear and nonlinear discriminant analysis, *J. Earth Sci.* **25**, 140–145, doi: [10.1007/s12583-014-0406-x](https://doi.org/10.1007/s12583-014-0406-x).
- Li, Y., X. Chen, and L. Fu (2012). Temporal and spatial variation of focal dynamic parameters in southwest Yunnan before the 2007 Ms6.4 Ning'er earthquake, *Earthquake* **32**, 28–39, doi: [10.3969/j.issn.1000-3274](https://doi.org/10.3969/j.issn.1000-3274).
- Linville, L., K. Pankow, and T. Draelos (2019). Deep learning models augment analyst decisions for event discrimination, *Geophys. Res. Lett.* **46**, 3643–3651, doi: [10.1029/2018gl081119](https://doi.org/10.1029/2018gl081119).
- Long, J., E. Shelhamer, and T. Darrell (2015). Fully convolutional networks for semantic segmentation, *IEEE Trans. Pattern. Anal. Mach. Intell.* **39**, 3431–3440, doi: [10.1109/TPAMI.2016.2572683](https://doi.org/10.1109/TPAMI.2016.2572683).
- Miao, F., N. S. Carpenter, Z. Wang, A. S. Holcomb, and E. W. Woolery (2020). High-accuracy discrimination of blasts and earthquakes using neural networks with multiwindow spectral data, *Seismol. Res. Lett.* **91**, 1646–1659, doi: [10.1785/0220190084](https://doi.org/10.1785/0220190084).
- Naresh, K., and N. Duraipandian (2021). Malicious traffic classification using long short-term memory (LSTM) model, *Wireless Pers. Comm.* doi: [10.21203/rs.3.rs-159180/v1](https://doi.org/10.21203/rs.3.rs-159180/v1).
- Nguyen, H., X.-N. Bui, H.-B. Bui, and D. T. Cuong (2019). Developing an XGBoost model to predict blast-induced peak particle velocity in an open-pit mine: A case study, *Acta. Geophysica* **67**, 477–490, doi: [10.1007/s11600-019-00268-4](https://doi.org/10.1007/s11600-019-00268-4).
- O'Rourke, C. T., G. E. Baker, and A. F. Sheehan (2016). Using P/S amplitude ratios for seismic discrimination at local distances, *Bull. Seismol. Soc. Am.* **106**, 2320–2331, doi: [10.1785/0120160035](https://doi.org/10.1785/0120160035).
- Parsa, A. B., A. Movahedi, H. Taghipour, S. Derrible, and A. K. Mohammadian (2020). Toward safer highways, application of XGBoost and SHAP for real-time accident detection and feature analysis, *Accident. Anal. Prev.* **136**, 105,405, doi: [10.1016/j.aap.2019.105405](https://doi.org/10.1016/j.aap.2019.105405).
- Pitarka, A., R. J. Mellors, W. R. Walter, S. Ezzedine, O. Vorobiev, T. Antoun, J. L. Wagoner, E. M. Matzel, S. R. Ford, A. J. Rodgers, et al. (2015). Analysis of ground motion from an underground chemical explosion, *Bull. Seismol. Soc. Am.* **105**, 2390–2410, doi: [10.1785/0120150066](https://doi.org/10.1785/0120150066).
- Pomeroy, P. W., W. J. Best, and T. V. McEvilly (1982). Test ban treaty verification with regional data: A review, *Bull. Seismol. Soc. Am.* **72**, S89–S129, doi: [10.1785/BSSA07206B0089](https://doi.org/10.1785/BSSA07206B0089).
- Pyle, M. L., and W. R. Walter (2019). Investigating the effectiveness of P/S amplitude ratios for local distance event discrimination, *Bull. Seismol. Soc. Am.* **109**, 1071–1081, doi: [10.1785/0120180256](https://doi.org/10.1785/0120180256).
- Qi, C., A. Fourie, X. Du, and X. Tang (2018). Prediction of open stope hangingwall stability using random forests, *Nat. Hazards* **92**, doi: [10.1007/s11069-018-3246-7](https://doi.org/10.1007/s11069-018-3246-7).
- Qi, C., A. Fourie, G. Ma, X. Tang, and X. Du (2018). Comparative study of hybrid artificial intelligence approaches for predicting hangingwall stability, *J. Comput. Civ. Eng.* **32**, doi: [10.1061/\(asce\)cp.1943-5487.0000737](https://doi.org/10.1061/(asce)cp.1943-5487.0000737).
- Randall, R. B. (2017). A history of cepstrum analysis and its application to mechanical problems, *Mech. Syst. Signal Process.* **97**, 3–19, doi: [10.1016/j.ymssp.2016.12.026](https://doi.org/10.1016/j.ymssp.2016.12.026).
- Renouard, A., A. Maggi, M. Grunberg, C. Doubre, and C. Hibert (2021). Toward false event detection and quarry blast versus earthquake discrimination in an operational setting using semiautomated machine learning, *Seismol. Res. Lett.* **92**, 3725–3742, doi: [10.1785/0220200305](https://doi.org/10.1785/0220200305).
- Reynen, A., and P. Audet (2017). Supervised machine learning on a network scale: Application to seismic event classification and detection, *Geophys. J. Int.* **210**, 1394–1409, doi: [10.1093/gji/ggx238](https://doi.org/10.1093/gji/ggx238).
- Ross, Z. E., M.-A. Meier, E. Hauksson, and T. H. Heaton (2018). Generalized seismic phase detection with deep learning, *Bull. Seismol. Soc. Am.* **108**, 2894–2901, doi: [10.1785/0120180080](https://doi.org/10.1785/0120180080).
- Samui, P. (2008). Slope stability analysis: A support vector machine approach, *Environ. Geol.* **56**, 255–267, doi: [10.1007/s00254-007-1161-4](https://doi.org/10.1007/s00254-007-1161-4).
- Smith, A. T. (1993). Discrimination of explosions from simultaneous mining blasts, *Bull. Seismol. Soc. Am.* **83**, 160–179, doi: [10.1785/BSSA0830010160](https://doi.org/10.1785/BSSA0830010160).
- Song, K., F. Yan, T. Ding, L. Gao, and S. Lu (2020). A steel property optimization model based on the XGBoost algorithm and improved PSO, *Comput. Mater. Sci.* **174**, doi: [10.1016/j.commatsci.2019.109472](https://doi.org/10.1016/j.commatsci.2019.109472).
- Stump, B. W., F. Rivirre-Barbier, I. Chernoby, and K. Koch (1994). Monitoring a Test Ban Treaty presents scientific challenges, *Eos Trans. AGU* **75**, 265–273, doi: [10.1029/94EO00940](https://doi.org/10.1029/94EO00940).
- Szegedy, C., V. Vanhoucke, S. Ioffe, J. Shlens, and Z. Wojna (2016). Rethinking the inception architecture for computer vision, *Proc. of the IEEE Conf. on Computer Vision and Pattern Recognition*, 2818–2826.
- Tang, L., M. Zhang, and L. Wen (2020). Support vector machine classification of seismic events in the Tianshan orogenic belt, *J. Geophys. Res.* **125**, e2019JB018132, doi: [10.1029/2019JB018132](https://doi.org/10.1029/2019JB018132).
- Tang, Z., Q. Liu, M. Wu, W. Chen, and J. Huang (2021). WiFi CSI gesture recognition based on parallel LSTM-FCN deep space-time neural network, *China Commun.* **3**, 205–215, doi: [10.23919/JCC.2021.03.016](https://doi.org/10.23919/JCC.2021.03.016) (in Chinese).
- Thomson, D. J. (1982). Spectrum estimation and harmonic analysis, *Proc. IEEE* **70**, 1055–1096, doi: [10.1109/PROC.1982.12433](https://doi.org/10.1109/PROC.1982.12433).
- Thomson, D. J. (2007). Jackknifing multitaper spectrum estimates, *IEEE Signal Proc Mag.* **24**, 20–30, doi: [10.1109/MSP.2007.4286561](https://doi.org/10.1109/MSP.2007.4286561).
- Um, T. T., F. Pfister, D. Pichler, S. Endo, M. Lang, S. Hirche, U. Fietzek, and D. Kulić (2017). Data augmentation of wearable sensor data for Parkinson's disease monitoring using convolutional neural networks, *ACM*, doi: [10.1145/3136755.3136817](https://doi.org/10.1145/3136755.3136817).
- Vapnik, V. (1995). *The Nature of Statistical Learning Theory*, SpringerVerlag, New York.
- Walter, W. R., D. A. Dodge, G. Ichinose, S. C. Myers, M. E. Pasano, and S. R. Ford (2018). Body-wave methods of distinguishing between explosions, collapses, and earthquakes: Application to recent events in North Korea, *Seismol. Res. Lett.* **89**, 2131–2138, doi: [10.1785/0220180](https://doi.org/10.1785/0220180).

- Wang, F., J. Yu, Z. Liu, M. Kong, and Y. Wu (2021). Study on offshore seabed sediment classification based on particle size parameters using XGBoost algorithm, *Comput. Geosci.* **149**, 104,713, doi: [10.1016/j.cageo.2021.104713](https://doi.org/10.1016/j.cageo.2021.104713).
- Wang, T., Y. Bian, Q. Yang, and M. Ren (2021). Correction of P/S amplitude ratios for low-magnitude seismic events based on Bayesian Kriging method, *Bull. Seismol. Soc. Am.* **111**, 2799–2813, doi: [10.1785/0120200293](https://doi.org/10.1785/0120200293).
- Wang, T., Z. Liu, T. Zhang, B. Liu, and Y. Li (2021). Time series classification based on Mixup data augmented LSTM-FCN, *Appl. Sci. Technol.* doi: [10.11991/yykj.202105006](https://doi.org/10.11991/yykj.202105006) (in Chinese).
- Wang, T. T., Y. J. Bian, and B. Zhang (2013). The comprehensive identification methods between earthquakes and explosions, *Prog. Geophys.* **28**, 2433–2443, doi: [10.6038/pg20130522](https://doi.org/10.6038/pg20130522) (in Chinese).
- Wei, Y. G., Q. L. Yang, T. T. Wang, C. S. Jiang, and Y. J. Bian (2019). Earthquake and explosion identification based on deep learning residual network model, *Acta Seismol. Sin.* **41**, 646–657, doi: [10.11939/jass.20190030](https://doi.org/10.11939/jass.20190030) (in Chinese).
- Woellmer, M., M. Kaiser, F. Eyben, B. Schuller, and G. Rigoll (2013). LSTM-modeling of continuous emotions in an audiovisual affect recognition framework, *Image. Vis. Comput.* **31**, 153–163, doi: [10.1016/j.imavis.2012.03.001](https://doi.org/10.1016/j.imavis.2012.03.001).
- Zhang, Y., T. Wang, Y. Bian, and Q. Yang (2021). Features of different types of seismic events in China's capital region, *Earthq. Sci.* **34**, 489–506, doi: [10.29382/eqs-2021-0035](https://doi.org/10.29382/eqs-2021-0035).
- Zhao, M., and S. Chen (2019). Waveform classification and seismic recognition by convolution neural network, *Chin. J. Geophys.* **62**, 374–382, doi: [10.6038/cjg2019M0151](https://doi.org/10.6038/cjg2019M0151) (in Chinese).
- Zhao, L., X. Xie, W. Wang, N. Fan, X. Zhao, and Z. Yao (2017). The 9 September 2016 north Korean underground nuclear test, *Bull. Seismol. Soc. Am.* **107**, 3044–3051, doi: [10.1785/0120160355](https://doi.org/10.1785/0120160355).
- Zhao, Y., L. Weihong, and G. Yanlin (1995). Distinguishing earthquake, explosion and mine earthquake in Beijing area, *Seismol. Geomagn. Observ. Res.* **16**, 48–54 (in Chinese).
- Zheng, X. F., Z. X. Yao, J. H. Liang, and S. X. Xu (2010). The role played and opportunities provided by IGP DMC of China National Seismic Network in Wenchuan earthquake disaster relief and researches, *Bull. Seismol. Soc. Am.* **100**, 2866–2872, doi: [10.1785/0120090257](https://doi.org/10.1785/0120090257).
- Zhou, J., Y. Yin, and B. Xia (2021). Acoustic emission signal recognition based on long short time memory neural network, *Comput. Sci.* **48**, 319–326, doi: [10.11896/jsjkx.210700034](https://doi.org/10.11896/jsjkx.210700034) (in Chinese).

Manuscript received 21 February 2022

Published online 23 November 2022